

Session 3

High performance simulation of plasma transport and validation

(Garrigues, Taccogna, Eremin, Powis, Knoll, Fubiani)



**ExB Plasmas
Workshop
2022**

Madrid, online event

List of contents

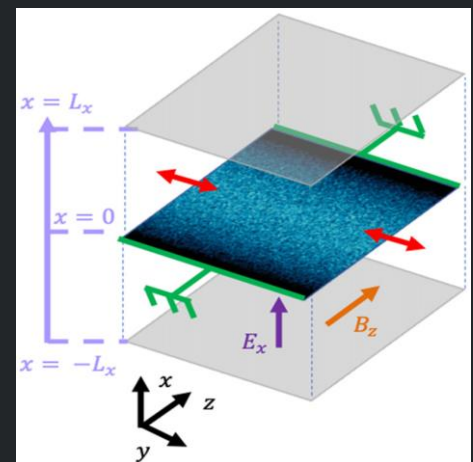
1. Common presentation

- Accelerating PIC simulations:
 - Eremin GPU-based
 - Minelli-Cichocki-Taccogna Hybrid MPI-OpenMP
 - Garrigues et al. Sparse PIC approach
 - Knoll et al. Dimensional reduction method
- Penning discharge benchmark: Powis-Garrigues-Fubiani

2. Discussion: validation of PIC simulations

D. Eremin, Parallelization of 2D and 3D PIC on CPU/GPU Platforms

(r, θ)



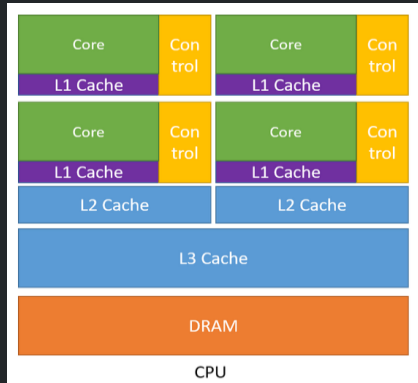
RUB	LAPLACE
CUDA C + C	Fortran
CUDA	MPI/OpenMP
Particle	Particle
Structured	Structured
NVIDIA Volta (GPU)	Intel Skylake
+ Intel Skylake (CPU)	
5120 cores (GPU)	2 \times 18 cores/node
+ 10 cores (CPU)	
@ 1.5 GHz–32 GB (GPU)	@ 2.30 GHz–64 GB
+ @ 2.2 GHz–96 GB (CPU)	
Explicit	Explicit
FFT + Thomas	PARDISO
2	2
1	1
Single*	Single*
Double**	Double**
11 h (1 GPU + 1 CPU)	12 h (180 CPU)
14 h (1 GPU + 1 CPU)	17 h (180 CPU)
29 h (1 GPU + 1 CPU)	27 h (180 CPU)

RUB code's parallelization strategies:

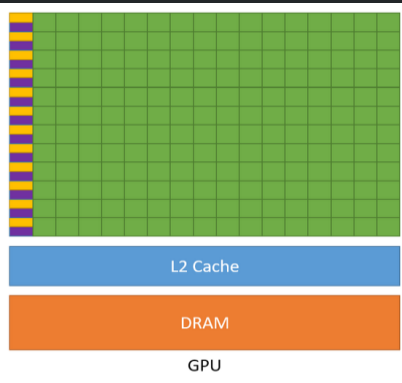
- Single-CPU/single-GPU heterogenous parallelization
- GPU: pusher, particle sorting, calculation of ρ and its Fourier decomposition, inverse Fourier transform of ϕ ; **particle decomposition** (CUDA C, each particle is processed by a separate GPU thread)
- CPU: 1D Poisson equation for each Fourier harmonic of ϕ Corresponding Thomas algorithm is extremely efficient
- **Mixed-precision approach** (single precision for particles, double precision for Poisson)

D. Eremin, Parallelization of 2D and 3D PIC on CPU/GPU Platforms

Architecture: CPU vs GPU

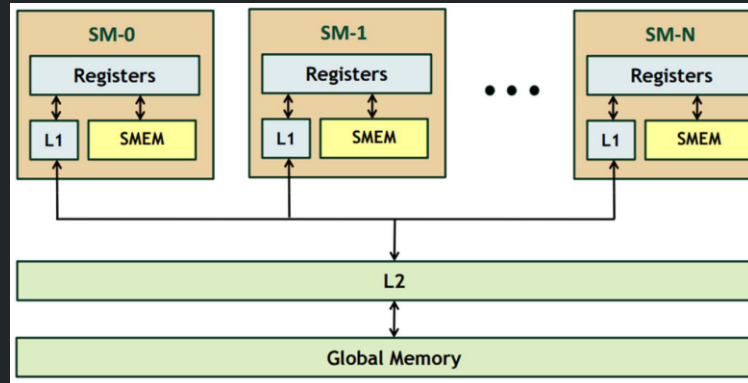


Latency-oriented architecture



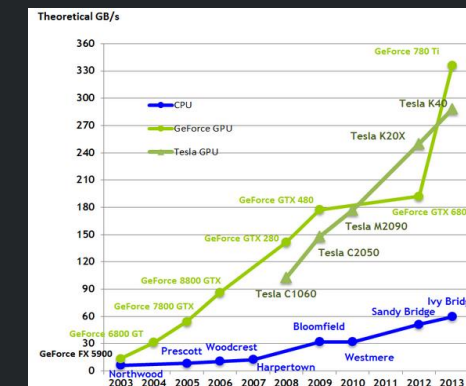
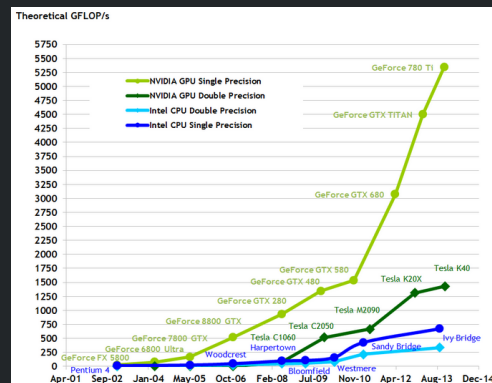
Throughput-oriented architecture

GPU memory system



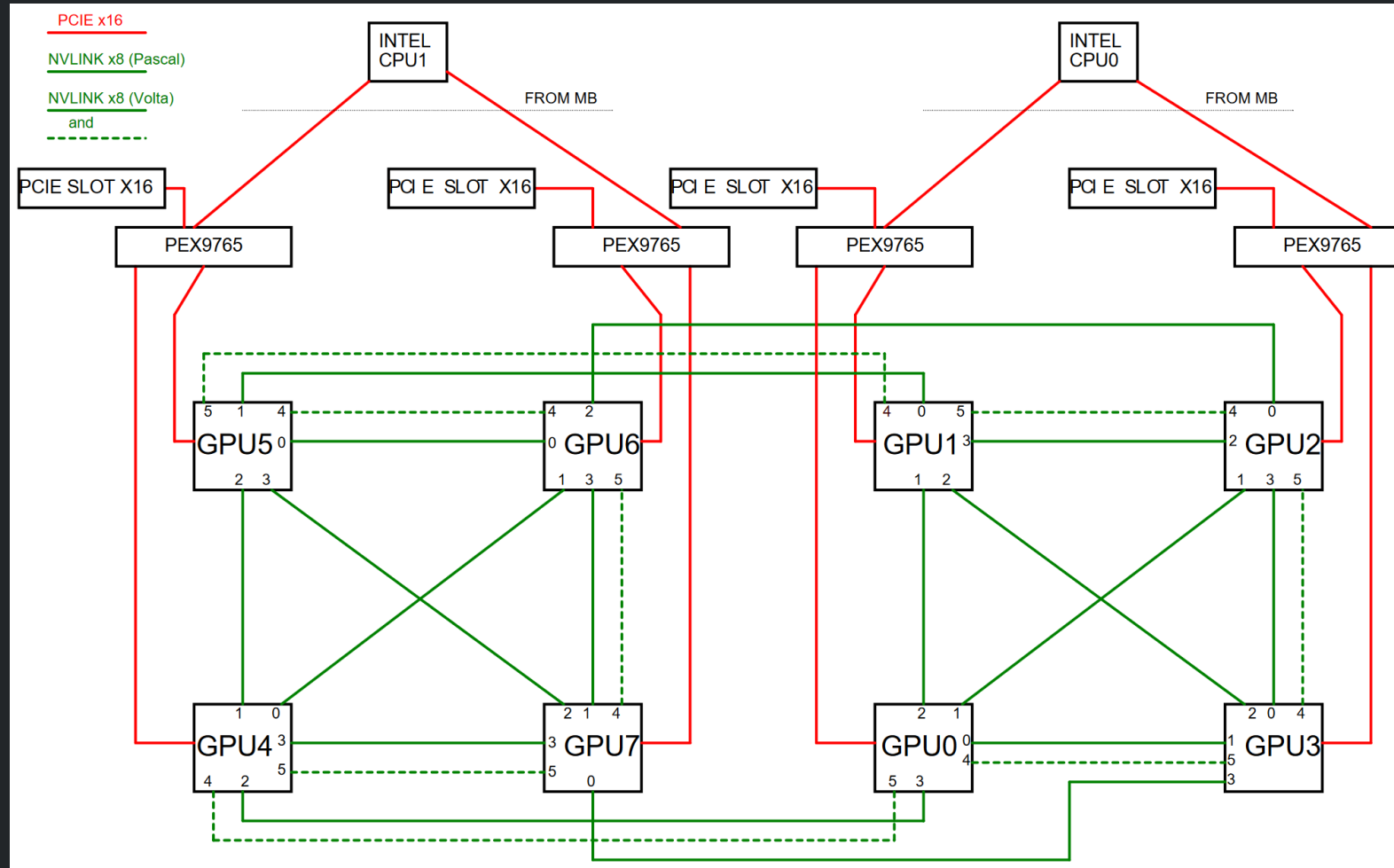
- Has fewer compatibility requirements compared to CPU (bold technological innovations are possible, e.g., HBM)
- Exposes many more memory types compared to CPU, which allows data reuse to hide the DRAM latency

Arithmetical and memory performance: CPU vs GPU



D. Eremin, Parallelization of 2D and 3D PIC on CPU/GPU Platforms

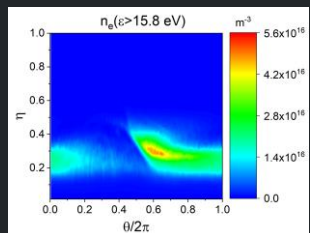
Typical server architecture featuring NVLink-connected GPUs



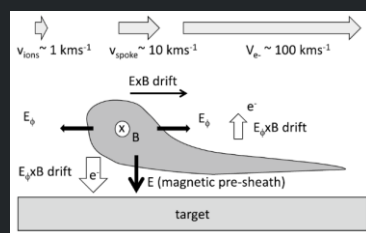
D. Eremin, Parallelization of 2D and 3D PIC on CPU/GPU Platforms

2D (θ, z) simulations of spokes in dcMS

PIC simulations

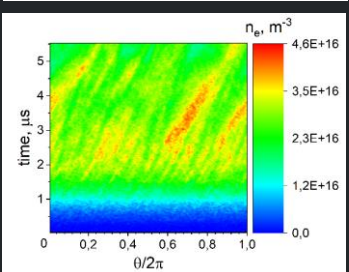
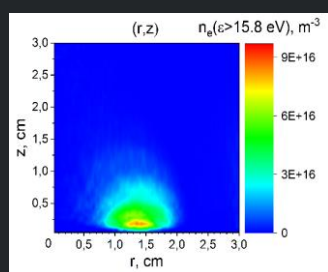
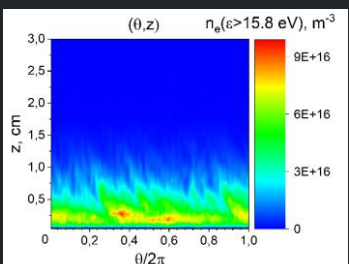
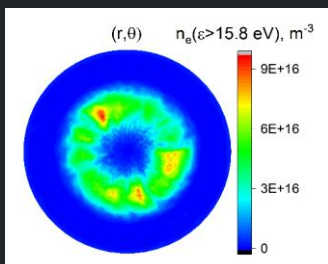


Expectation from experiments



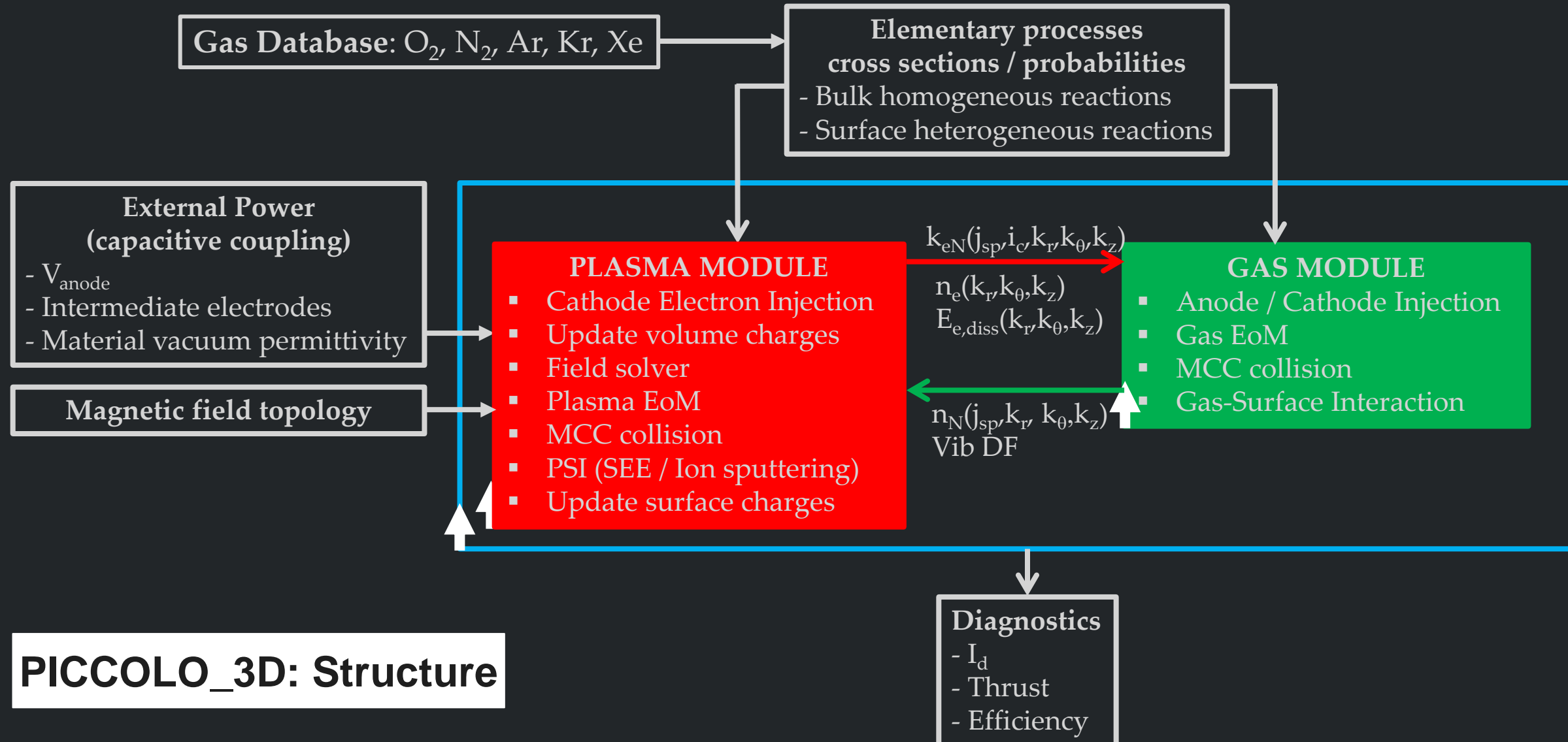
[J. Held and
A. von Keudell,
2020]

3D simulations of rotating instabilities



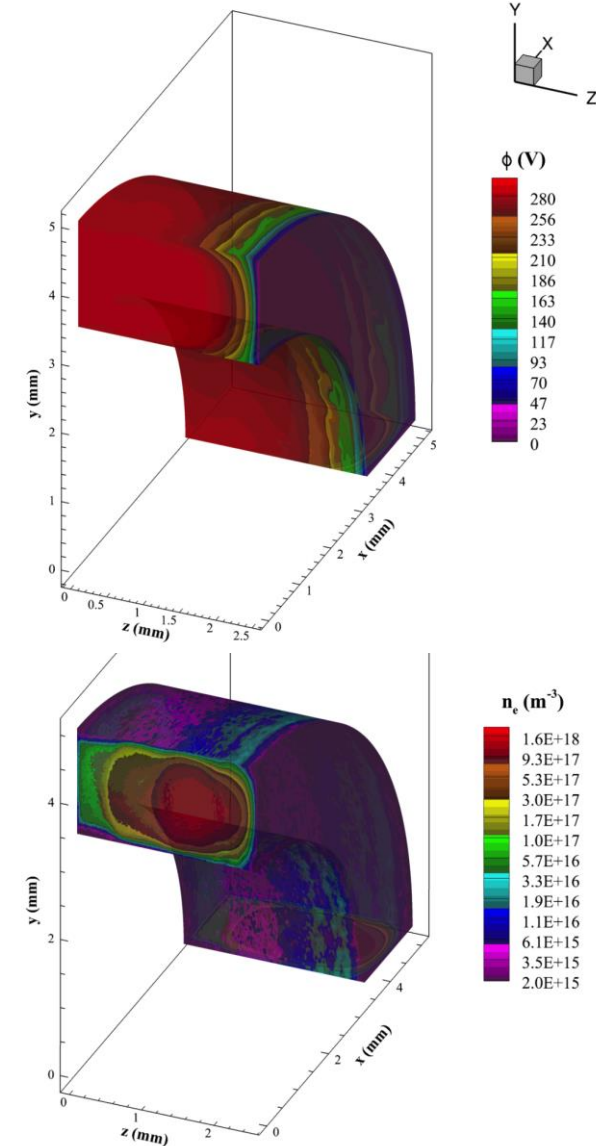
RUB 3D code's parallelization strategies:

- Single-CPU/multi-GPU heterogenous parallelization, domain decomposition in the z direction
- GPU: pusher, particle sorting, calculation of ρ and its Fourier decomposition, inverse Fourier decomposition of ϕ ; **particle decomposition** (CUDA C, each particle is processed by a separate GPU thread)
- CPU: 2D Poisson equation for each Fourier harmonic of ϕ ; **Fourier decomposition** (openMP, each potential harmonic is solved with multigrid algorithm by a separate CPU thread)
- **Mixed-precision approach**
(single precision for particles, double precision for Poisson)
Big potential for the mixed-precision parallelization of the multigrid solver on GPUs with tensor cores



PICCOLO_3D description:

- 3D cylindrical metrics including part of the plume
- SPT100 case: $N_g = 500 \times 300 \times 128$ grid nodes with $N_p = 2 \times 10^9$ total number of charged particles
- Domain decomposition with MPI framework:
 - decomposed in sub-domains of equal length along the azimuthal direction to minimize load imbalance
 - all the cells and particles of each sub-domain are assigned to a single MPI task
- Further domain decomposition by tiling to improve L2 cache use
- Particle decomposition inside each subdomain with OpenMP strategy
- Particle-based quantities: use of array of structures of arrays to speed up access to memory and to optimize OpenMP implementation
- Optimized and vectorized charge deposition and field gathering
- Particle sorting algorithm
- Ion orbit averaging subcycling



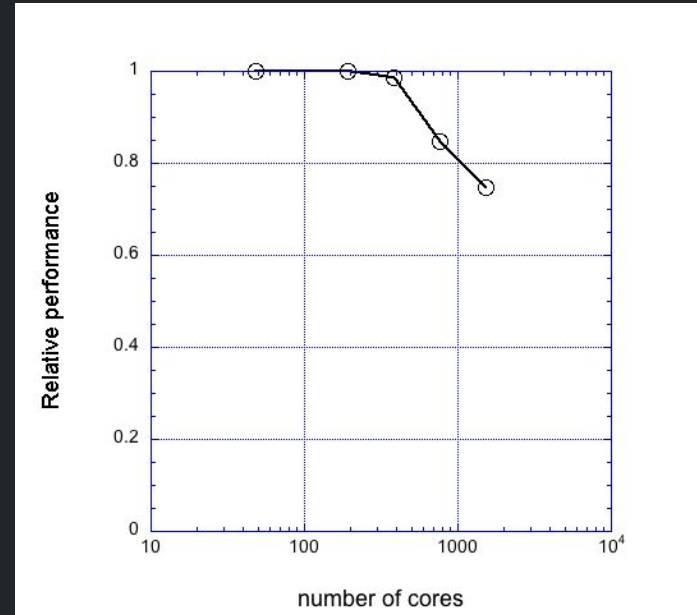
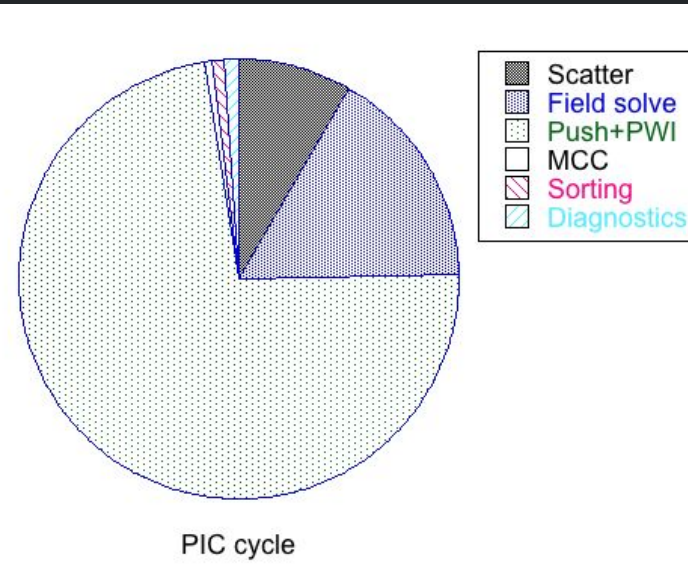
PICCOLO_3D: scaling performances

- Push represents 70% of PIC cycle
- Good scaling up to 500 cores

@Marconi-Cineca

# cores	speedup	Relative performance
192	1.0000	1
384	1.9726	0.986
768	3.3854	0.846
1536	5.9660	0.746

Subroutine	Time (s)
Scatter	0.28
Field solve	0.56
Push + PWI	2.46
MCC	0.01
Particle sorting	0.03
Diagnostics (minimum)	0.04
Total (PIC cycle)	3.38



Garrigues, Sparse PIC Approach, Slide 1 - Constrains Explicit Standard PIC

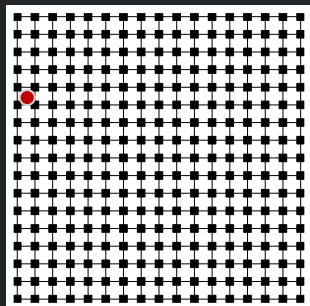
- Explicit PIC approach
 - Constrains of grid spacing and time step related to the resolution of electron properties (Debye length and inverse of plasma frequency)
 - Limitation to explicit PIC approach: high computational time due to exponential dependence on dimension

• **Sparse approach: reduction of dimension dependence for grid-based methods**

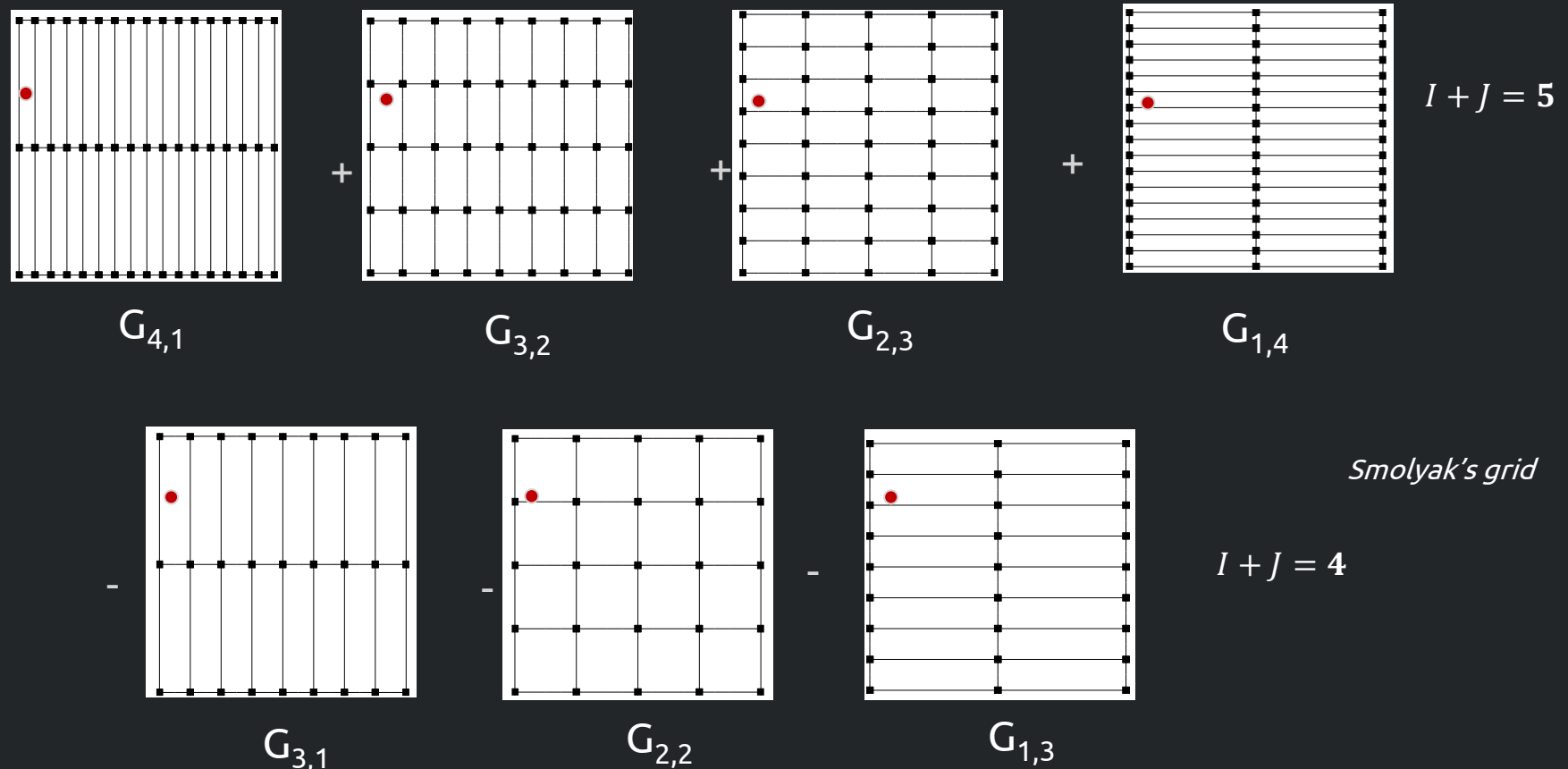
- Sparse grid techniques
 - Define a hierarchy of anisotropic grids with a coarser resolution
 - Reconstruction of the solution on the initial Cartesian grid using combination techniques
 - Preserving second order approximation (for $d > 1$)
 - Applied to Eulerian approaches
 - Applied to PIC approaches: L. F. Ricketson and A. J. Cerfon, PPCF **59**, 024002 (2017), L. Garrigues et al., JAP **129**, 153303, ibid 153304 (2021)
 - Particle sampling error scales as same manner than the standard approach,
 - Using same NPC concept still relevant for Sparse PIC method as in standard approach

Garrigues, Sparse PIC Approach, Slide 2 - Grid Construction

16x16
 $2^n \times 2^n, n=4$



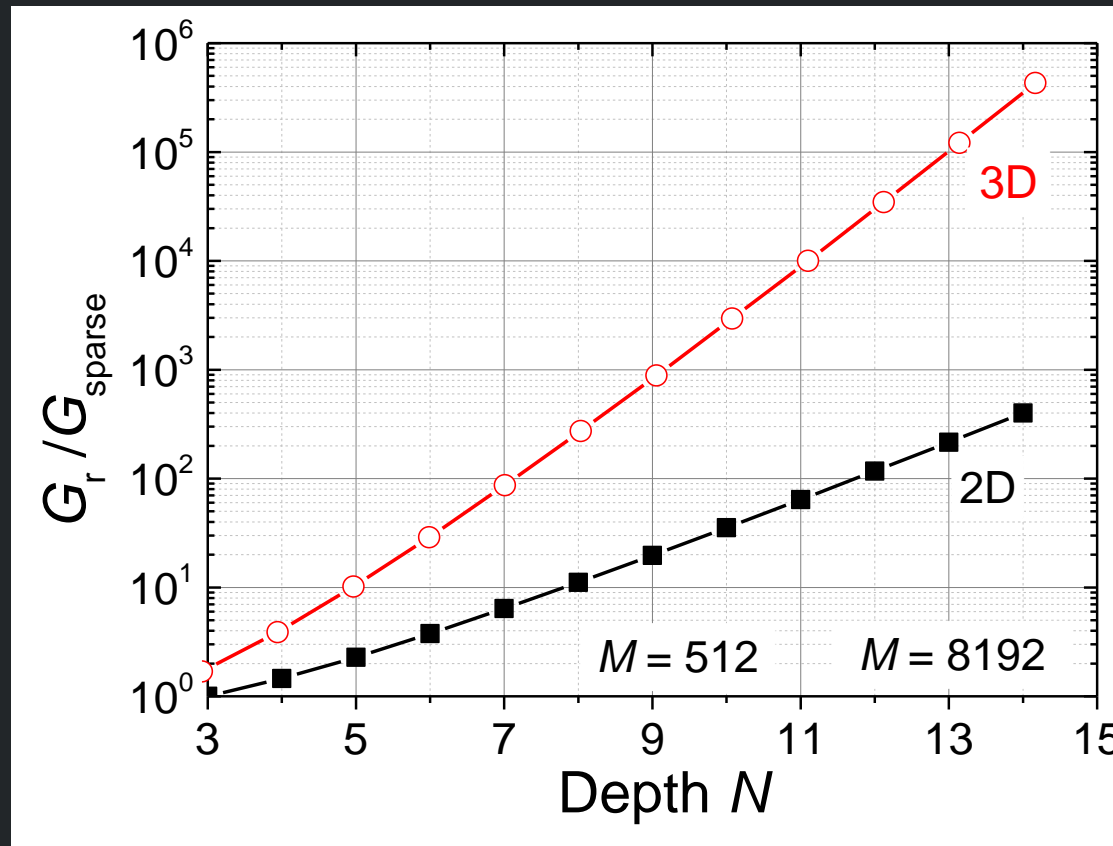
G_{regular}
 $\Delta x \sim \lambda_d$



Recombination technique

$$U_N = \sum_{I+J=N+1} U_{IJ} - \sum_{I+J=N} U_{IJ}$$

Garrigues, Sparse PIC Approach, Slide 3 - Reduction in the Number of Cells



Gain in number of cells, Gain in number of particles
Reduction of computational time

large speed up expected for 3D simulations

$$\{ \text{cells}(512^3) \}_{\text{sparse}}$$

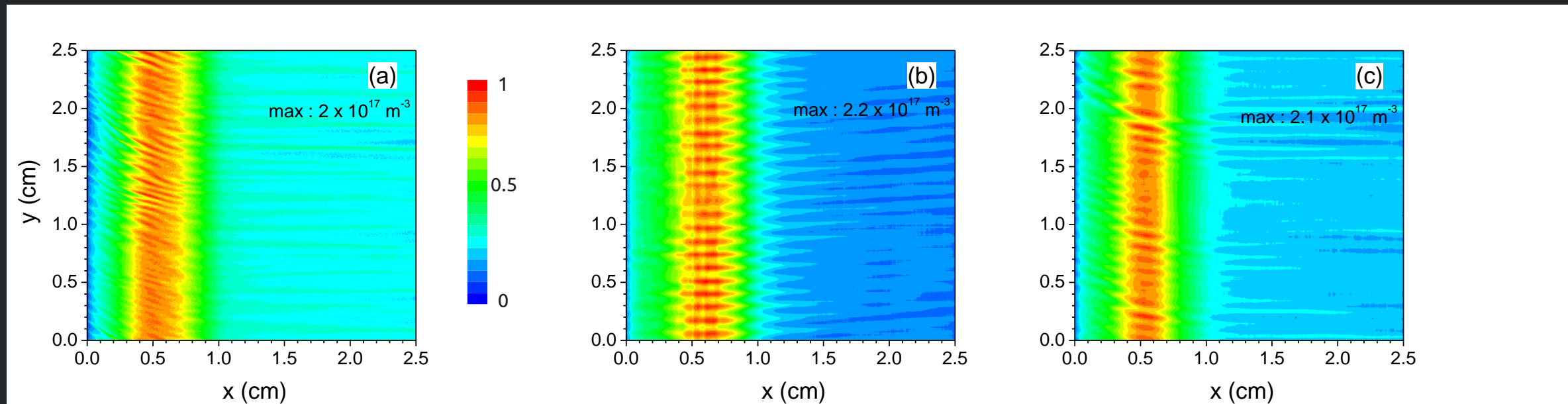
$$< \{ \text{cells}(512^2) \}_{\text{standard}}$$

$$\{ \text{cells}(512^2) \}_{\text{sparse}}$$

$$= \{ \text{cells}(512^2) \}_{\text{standard}} / 20$$

Garrigues, Sparse PIC Approach, Slide 4 - Illustration 2D - EDI – Hall thruster

- 2D EDI in the (x, θ) plane of a Hall thruster – Landmark project – Case 2b, T. Charoy et al., PSST, **28**, 105010 (2019)
- Ion density profile



Regular grid: 512×512
Npc: 400

Sparse, $N = 9$, standard
Npc: 400
Gain in comp. time: 6.5

Sparse, $N = 9$, more aniso.
Npc: 400
Gain in comp. time: 4

L. Garrigues et al., JAP **129**, 153304 (2021)

F. Deluzet et al., *submitted*

IPPL, Reduced-order PIC simulation, slide 1

- The **principal idea** behind the reduced-order PIC simulation is to **lower to 1D the dimensionality of the Poisson's equation** by taking integrals of the multi-dimensional equation **to obtain a coupled system of 1D ODEs** for the potential functions ϕ^x, ϕ^y , and ϕ^z .
- The **aim** is to **reduce the computational cost** of multi-dimensional PIC simulations **through significant reduction in the necessary total number of macroparticles**.
- This is done **by splitting the computational domain** into several “**Regions**” that meet the following criteria:
 - the **extent of the regions** (L_R) are **much larger than the Debye length** ($L_R \gg \lambda_D$), and,
 - **Within each region**, the gradient of the potential along each coordinate is more significant than its gradient along the other two perpendicular directions (**1D approximation**, e.g., $\frac{\partial\phi}{\partial x} \gg \frac{\partial\phi}{\partial y}, \frac{\partial\phi}{\partial z}$), **thus**, allowing to **assume** $\phi(x, y, z) = \phi^x(x) + \phi^y(y) + \phi^z(z)$.

To simplify the discussion, we look at the **formulation for a single region in a 2D domain**. We thus have:

$$\nabla^2 \phi(x, y) = \frac{\partial^2 \phi(x, y)}{\partial x^2} + \frac{\partial^2 \phi(x, y)}{\partial y^2} = -\frac{\rho(x, y)}{\epsilon_0}$$

$$\phi(x, y) = \phi_{n,m}^x(x) + \phi_{n,m}^y(y)$$

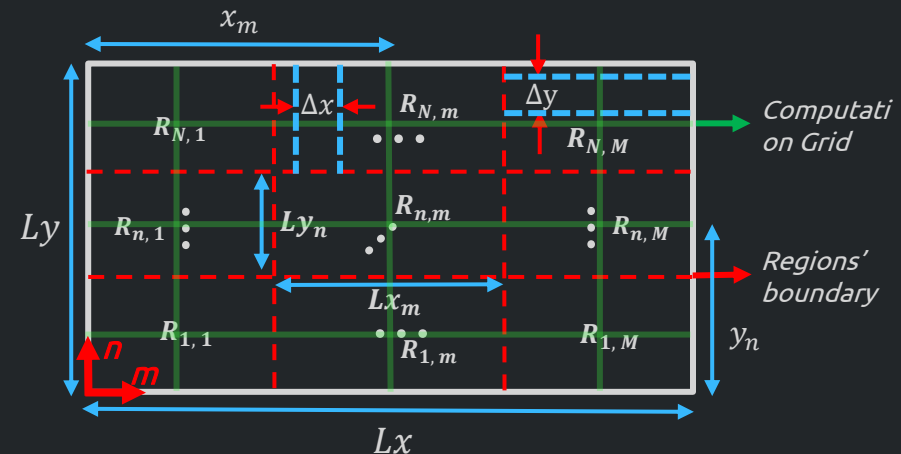
2D Poisson's Eq.

Q2D assumption (in each region)

Substituting in 2D equation

$$\left\{ \begin{array}{l} \frac{\partial^2 \phi_{n,m}^x(x)}{\partial x^2} L y_n + \frac{\partial \phi_{n,m}^y}{\partial y} \Big|_{y_n+L y_n/2} - \frac{\partial \phi_{n,m}^y}{\partial y} \Big|_{y_n-L y_n/2} = -\frac{1}{\epsilon_0} \int_{y_n-L y_n/2}^{y_n+L y_n/2} \frac{\rho(x, y)}{\epsilon_0} dy \\ \frac{\partial^2 \phi_{n,m}^y(y)}{\partial y^2} L x_m + \frac{\partial \phi_{n,m}^x}{\partial x} \Big|_{x_m+L x_m/2} - \frac{\partial \phi_{n,m}^x}{\partial x} \Big|_{x_m-L x_m/2} = -\frac{1}{\epsilon_0} \int_{x_m-L x_m/2}^{x_m+L x_m/2} \frac{\rho(x, y)}{\epsilon_0} dx \end{array} \right.$$

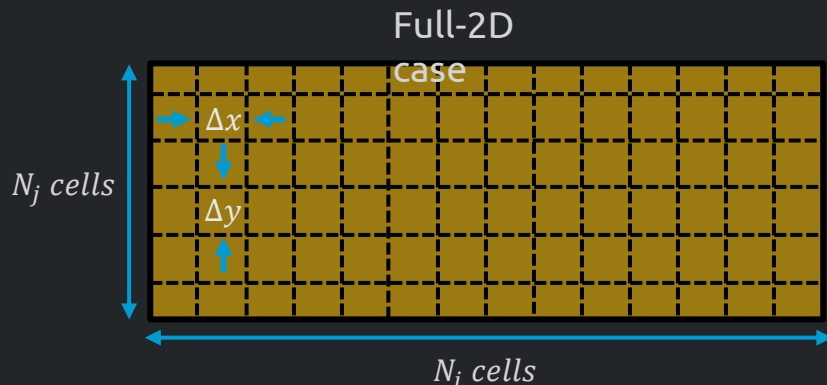
and integrating along the x and y extent of the regions



Schematics of the multi-region reduced-order PIC simulation in 2D configuration

IPPL, Reduced-order PIC simulation, slide 2

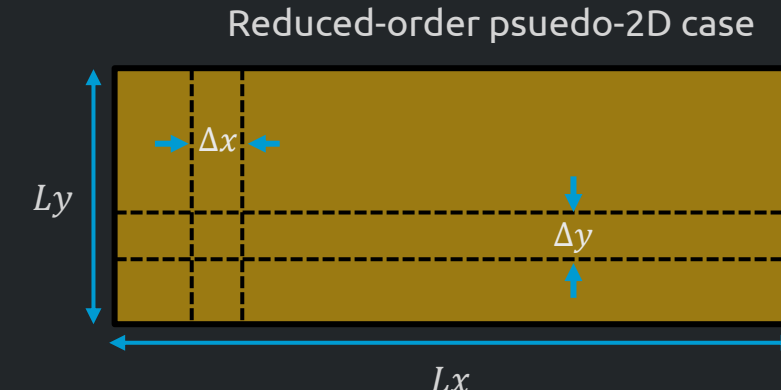
- Here, we demonstrate quantitatively the computational advantage that the approach has over traditional multi-dimensional PIC simulations, which essentially paves the way towards 3D approximation of the domain.
- For simplicity, we focus on an implementation where an entire 2D domain is approximated by a single region.



Total number of cells: $N_i \times N_j$

Typical minimum $N_{ppc} = 100$

Total $N_{p,initial} = 100 \times N_i \times N_j$



Total maximum number of cells: $\max(N_i, N_j)$

Typical minimum $N_{ppc} = 100$

Total maximum $N_{p,initial} = \max(100 \times N_i, 100 \times N_j)$

For a typical 500×250 2D domain, we have

$N_{p,initial} = 1.25 \times 10^7$ for full-2D case

$N_{p,initial} = 5 \times 10^4$ for the pseudo-2D case

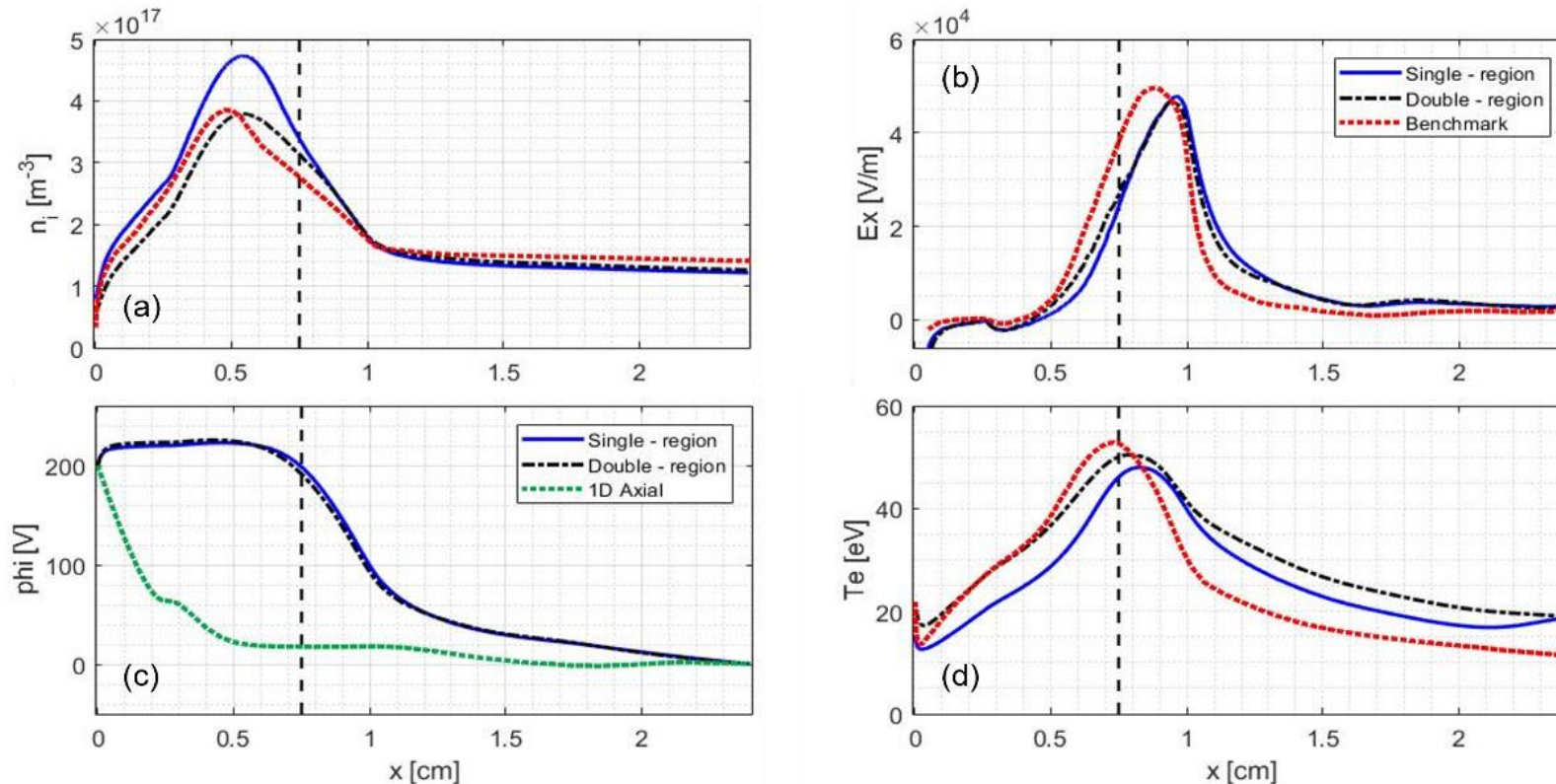


The reduced-order PIC simulation results in 250 times reduction in computational cost

IPPL, Reduced-order PIC simulation, slide 3

- Verification of the reduced-order PIC was performed in axial-azimuthal configuration (pseudo-2D simulation) using the single-and double-region implementations, taking as reference the full-2D $z - \theta$ benchmark results reported in T Charoy et al. 2019 *Plasma Sources Sci. Technol.* 28 105010.

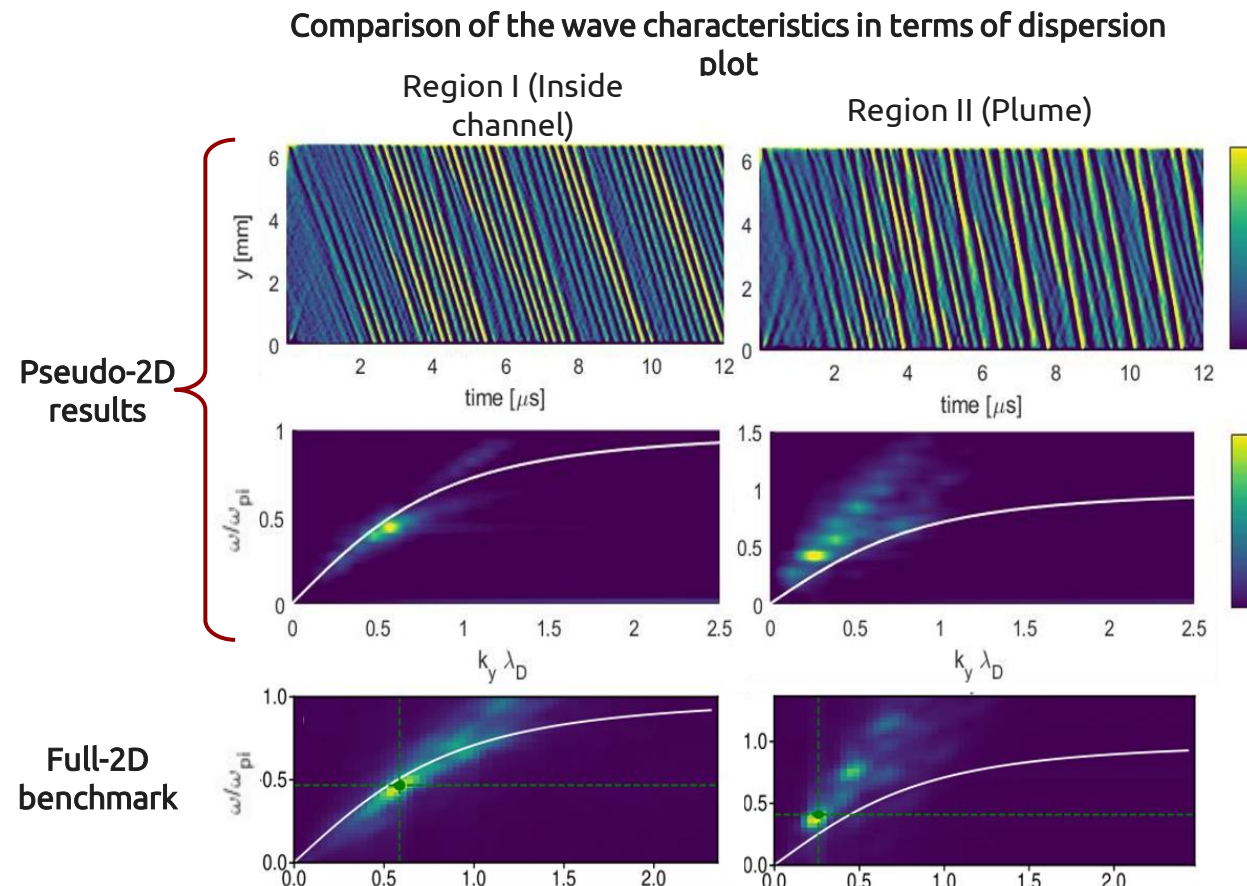
Time averaged axial profiles of plasma properties



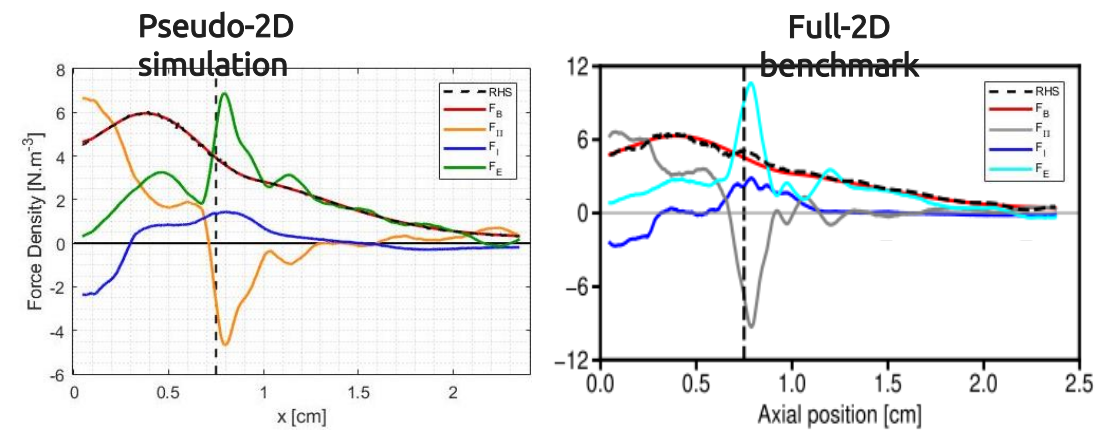
Plot (c) illustrates the capability of the pseudo-2D simulation to properly incorporate the necessary wave-induced mobility for the sustainment of plasma potential.

IPPL, Reduced-order PIC simulation, slide 4

- In addition to time-averaged plasma properties, the **pseudo-2D simulation is also capable of capturing accurately the azimuthal waves and their induced transport**, remarkably similar to the full-2D simulation.



Comparison of the contribution of force terms in electron azimuthal momentum equation to axial transport



$$-qn_e v_{e,x} B = \partial_t (mn_e v_{e,y}) + \partial_x (mn_e v_{e,x} v_{e,y}) + \partial_x (\Pi_{e,xy}) - qn_e E_y$$

\mathbf{F}_B \mathbf{F}_t \mathbf{F}_I \mathbf{F}_{Π} \mathbf{F}_E

List of references

- L. Garrigues, B. Tezenas du Montcel, G. Fubiani, F. Bertomeu, F. Deluzet, and J. Narski, “Application of Sparse Grid Combination Techniques to Low Temperature Plasmas Particle-In-Cell Simulations. I. Capacitively Coupled Radio Frequency Discharges”, J. Appl. Phys. 129, 153303 (2021) <https://doi.org/10.1063/5.0044363>
- L. Garrigues, B. Tezenas du Montcel, G. Fubiani, and B. Reman, “Application of Sparse Grid Combination Techniques to Low Temperature Plasmas Particle-In-Cell Simulations. II. Electron Drift Instability in a Hall thruster”, J. Appl. Phys. 129, 153304 (2021) <https://doi.org/10.1063/5.0044865>
- T. Charoy, J. P. Boeuf, A. Bourdon, J. A. Carlsson, P. Chabert, B. Cuenot, D. Eremin, L. Garrigues, K. Hara, I. D. Kaganovich, A. T. Powis, A. Smolyakov, D. Sydorenko, A. Tavant, O. Vermorel, and W. Villafana, “ 2D Axial-Azimuthal Particle-In-Cell Benchmark for Low-Temperature Partially Magnetized Plasmas”, Plasma Sources Sci. and Technol. 28, 105010 (2019) <https://doi.org/10.1088/1361-6595/ab46c5>
- L. F. Ricketson and A. J. Cerfon, “Sparse grid techniques for particle-in-cell schemes”, Plasma Phys. Control. Fusion 59, 024002 (2017) <https://doi.org/10.1088/1361-6587/59/2/024002>
- S. Muralikrishnan, A. J. Cerfon, M. Frey, L. F. Ricketson, and A. Adelmann, “Sparse Grids based Adaptive Noise Reduction strategy for Particle-In-Cell schemes”, <https://arxiv.org/abs/2008.09441>
- F. Deluzet, G. Fubiani, L. Garrigues, C. Guillet, and J. Narski, “Sparse Grid Reconstructions for Particle-In-Cell Methods” <https://hal.archives-ouvertes.fr/hal-03355720>
- W. Villafana, F. Petronio, A.C. Denig, M.J. Jimenez, D. Eremin, L. Garrigues, F. Taccogna, A. Alvarez-Laguna, J.P. Boeuf, A. Bourdon, P. Chabert, T. Charoy, B. Cuenot, K. Hara, F. Pechereau, A. Smolyakov, D. Sydorenko, A. Tavant and O. Vermorel, “2D radial-azimuthal particle-in-cell benchmark for E×B discharges ”, Plasma Sources Sci. Technol. 30 075002 (2021) <https://doi.org/10.1088/1361-6595/ac0a4a>
- D. Eremin, “An energy- and charge-conserving electrostatic implicit particle-in-cell algorithm for simulations of collisional bounded plasmas”, J. Comput. Phys. 452, 110934 (2022) <https://doi.org/10.1016/j.jcp.2021.110934>
- H. Vincenti, M. Lobet, R. Lehe, R. Sasanka, J.-L. Vay, ” An efficient and portable SIMD algorithm for charge/current deposition in Particle-In-Cell codes”, "Comput. Phys. Comm., 210, 145 (2017) <http://dx.doi.org/10.1016/j.cpc.2016.08.023>
- H. Vincenti, M. Lobet, R. Lehe, J.-L. Vay, J. Deslippe, ” "PIC codes on the road to exascale architectures”, Chapt. 17 in Exascale Scientific Applications: Scalability and Performance Portability, edited by Tjerk P. Straatsma, Katerina B. Antypas, Timothy J. Williams, CRC Press (2018)

Penning Discharge Benchmark

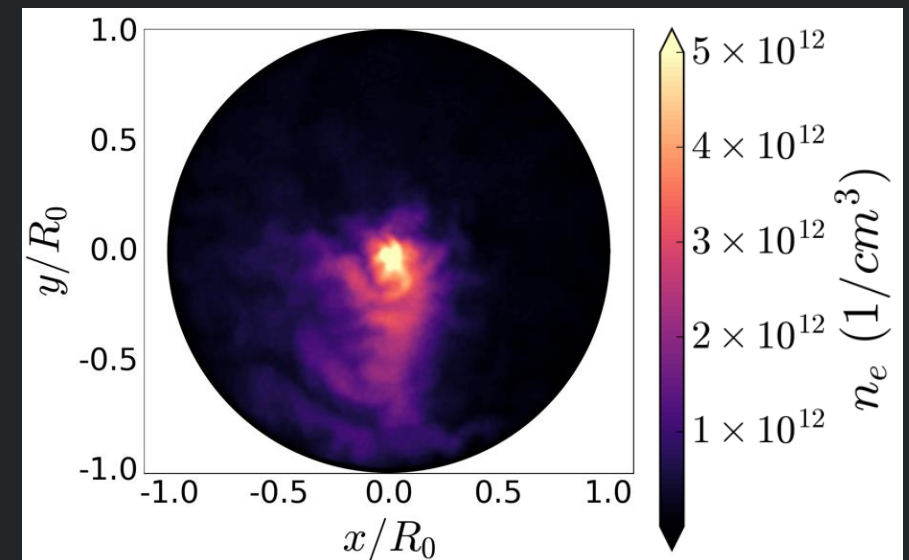
Andrew (Tasman) Powis, Laurent Garrigues, Gwenael Fubiani

Motivation – Code Benchmarking

- This proposed effort evolved from discussions following the highly successful Landmark 2a benchmark, Charoy *et al.* 2019
- The basis for the setup is the paper from *Powis et al.* 2018 which simulates the emergence of a large-scale coherent rotating structure within a Penning discharge.
- However there exist many simulation efforts which capture similar structures occurring within low-temperature partially magnetized ExB plasmas [1-9]

We propose two benchmark setups:

1. Collisionless case (the topic of this presentation):
 - a) Capture the emergence of large scale coherent structures as well as micro-turbulence in partially magnetized ExB plasmas
2. Collisional case:
 - a) This will extend benchmarking of code capabilities beyond that of Landmark 2a and the collisionless case considered here
 - b) We are still exploring the appropriate parameters to include in this case
 - c) The ad-hoc nature of MCC collision modules make it challenging to converge on a clear and concise problem description



Electron density plots demonstrating formation of a rotating spoke within 2D Penning discharge simulations [*Powis et al.* 2018]

Motivation – A Pathway to Validation

- Numerous past and current experiments exhibit spoke like phenomena, and several are designed to explicitly explore the structure:
 - Penning like or plasma columns (including Mistral) [10-15]
 - Hall thrusters [16-28]
 - Planar magnetrons [29-26]
 - Cylindrical magnetrons [37,38]
- From the simulation side, our pathway to validation against experiments is as follows:
 1. Benchmark 2D collisionless simulations (as proposed here)
 2. Benchmark 2D collisional simulations, with increasing addition of relevant reactions
 3. Work with experimentalists to determine appropriate conditions which are feasible for simulations and experiments
 4. Compare with experiments, add to models as required (i.e. complex boundary conditions, 3D geometry etc.) to reach agreement

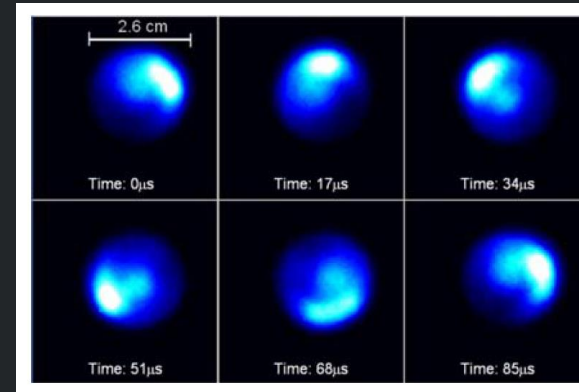
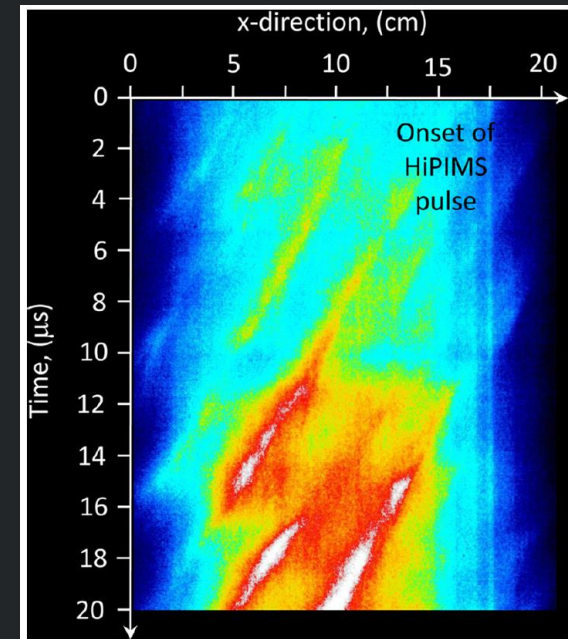


Photo-emission from a Xenon plasma rotating within a cylindrical Hall thruster [Raitses *et al.* 2012]



Spatio-temporal plots of photo-emission from Argon in a HiPIMS planar magnetron. Streaks indicate the presence of a spoke during a pulse [Anders *et al.* 2017]

Motivation – Unsolved Physics

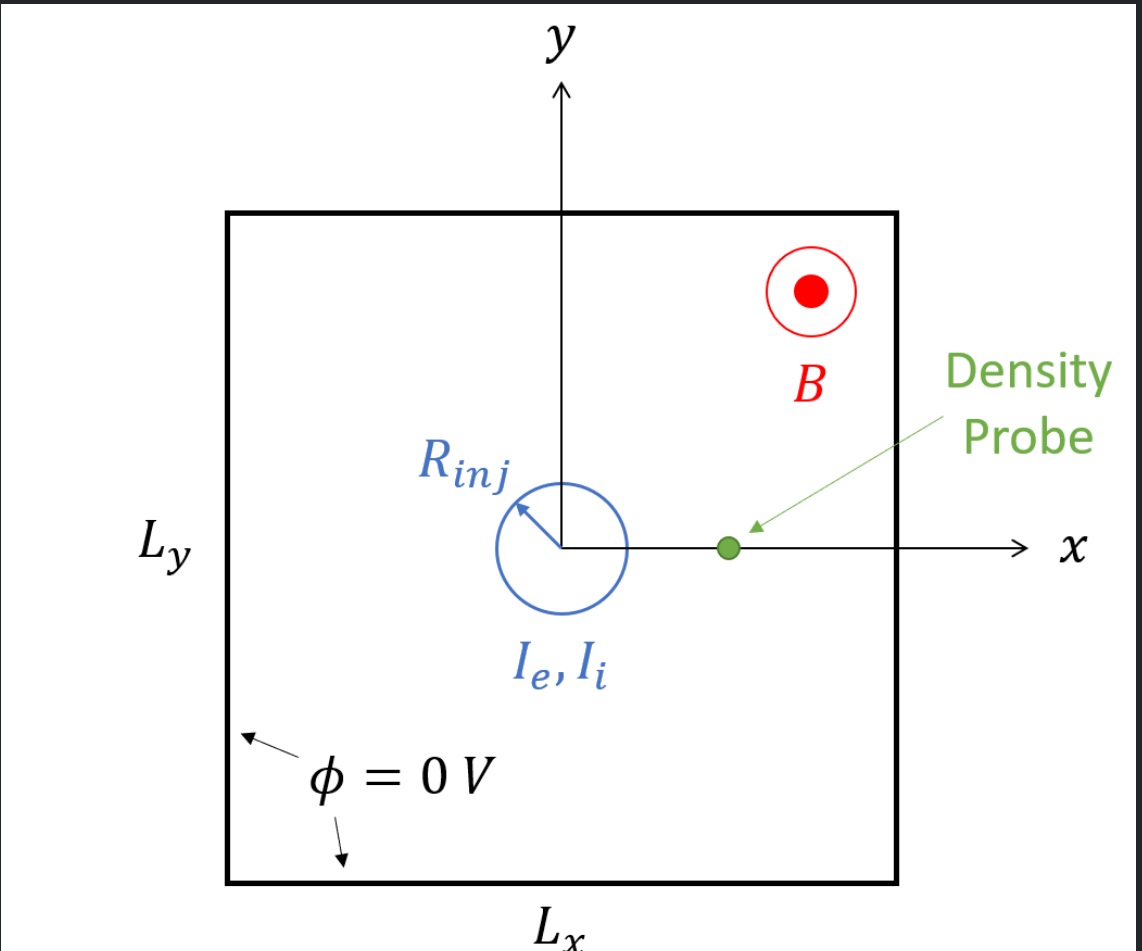
- Clearly the rotating spoke and associated anomalous transport have enjoyed a rich history of research
- This benchmark provides a pathway to engage more plasma physicists (both computational and experimental) to investigate this interesting and unsolved problem.
- Some interesting and unsolved questions include:
 - How does the spoke form? Is it a single coherent instability? Is it an inverse-cascade?
 - What are the characteristics of the micro-turbulence which forms within the spoke?
 - How does the spoke affect cross-field transport? Does it drive it directly or does turbulence within the structure promote transport? I.e., which wavenumbers are responsible for anomalous transport?
 - Can we control (or do we want to control) the spoke?

Problem Description 1

Properties of the simulation:

- 2D square domain supporting a uniform Cartesian grid with grounded walls
- Evolved for $500 \mu s$, sufficient for multiple rotations of the emergent spoke
- Uniform constant magnetic field applied in the z-direction (out of the page)
- The time step and cell size are sufficiently small to resolve the smaller electron plasma period and Debye length respectively

A complete description of the problem will be made available to all participants shortly.



Penning discharge benchmark simulation schematic

Problem Description 2

Emerging physics

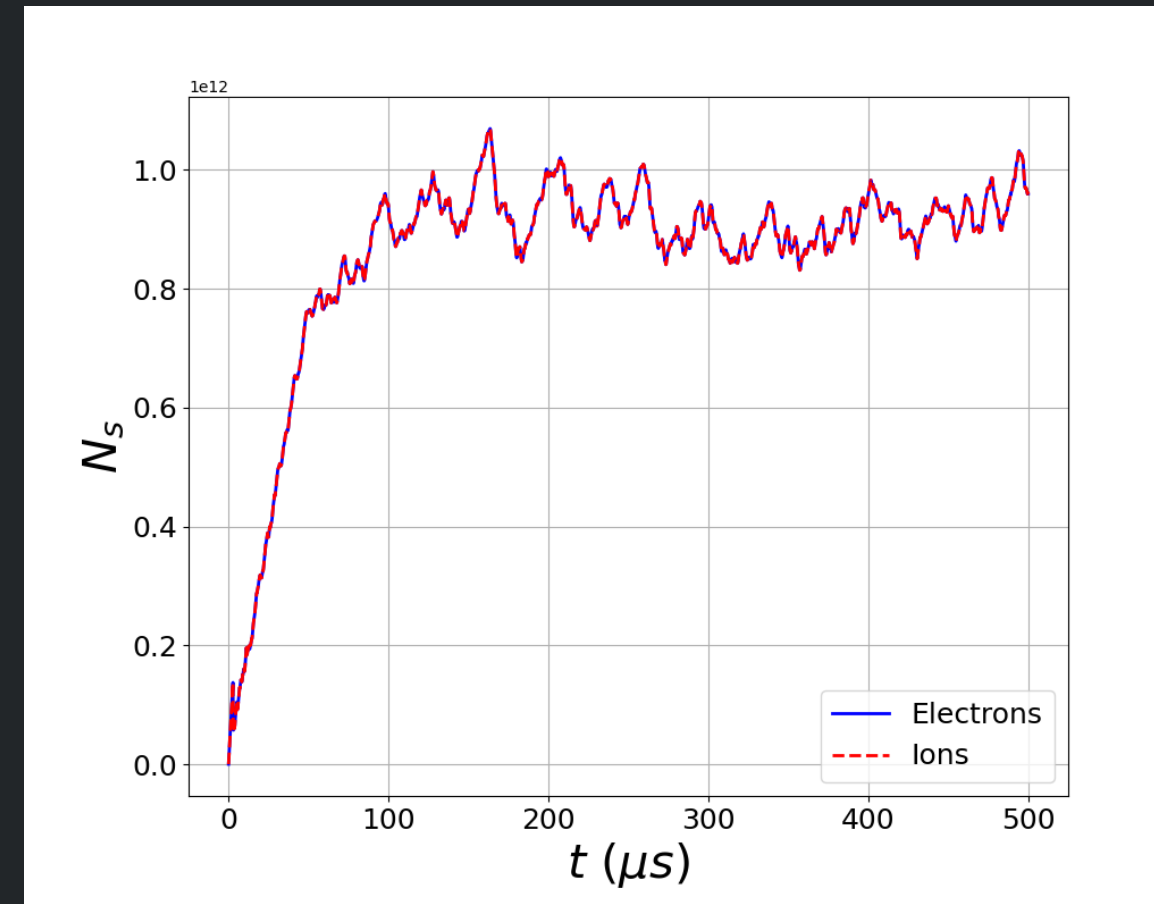
- The domain begins completely empty
- A constant current of ions and electrons are injected into the center
- The flux of electrons is higher than that of ions, therefore a negative potential builds up in the center forcing electron transport to the walls
- The system is non-neutral for up to $10 - 20 \mu s$
- The spoke emerges after around $50 - 100 \mu s$ and is presumably the most efficient structure to transport electrons from the center to the walls
- Quasi-steady state is achieved after $100 \mu s$

- MOVIE

Problem Description 3

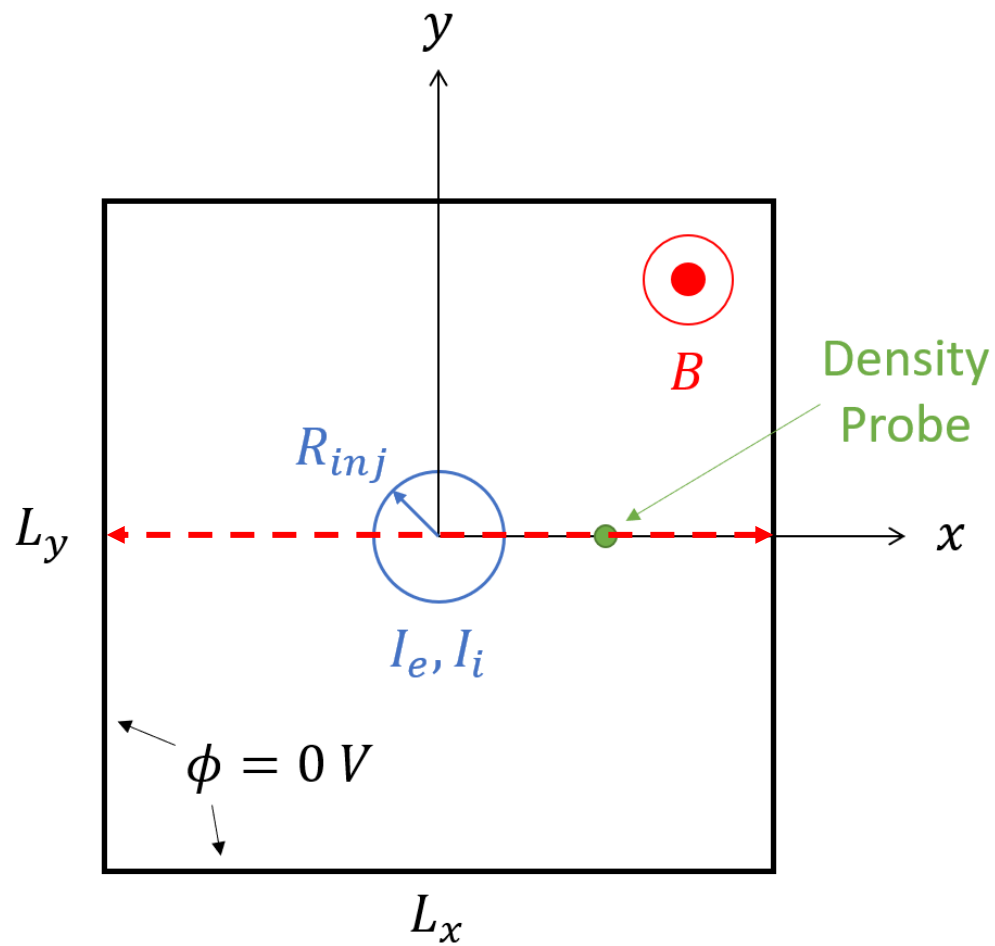
Emerging physics

- The domain begins completely empty
- A constant current of ions and electrons are injected into the center
- The flux of electrons is higher than that of ions, therefore a negative potential builds up in the center forcing electron transport to the walls
- The system is non-neutral for up to $10 - 20 \mu s$
- The spoke emerges after around $50 - 100 \mu s$ and is presumably the most efficient structure to transport electrons from the center to the walls
- Quasi-steady state is achieved after $100 \mu s$

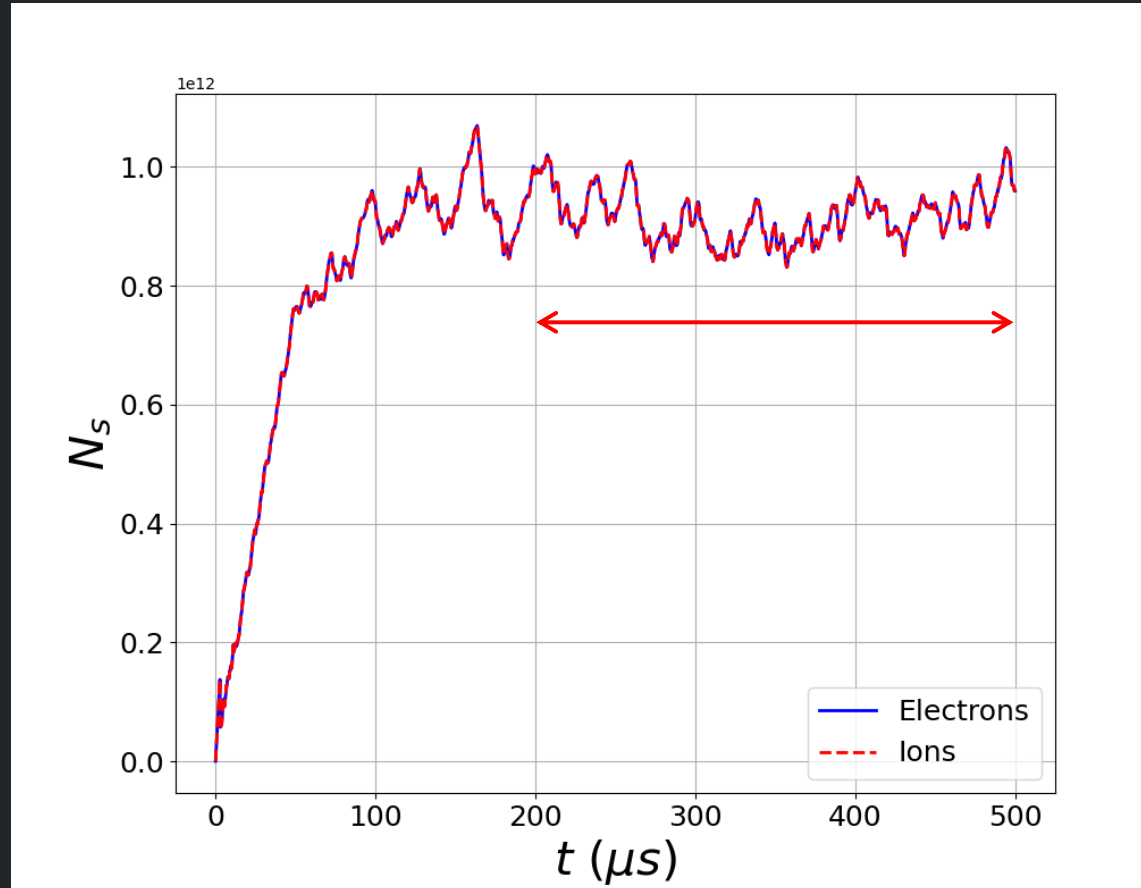


Total electrons and ions vs time within the entire simulation domain

Diagnostics – Time Averaged Cross-Section Profiles

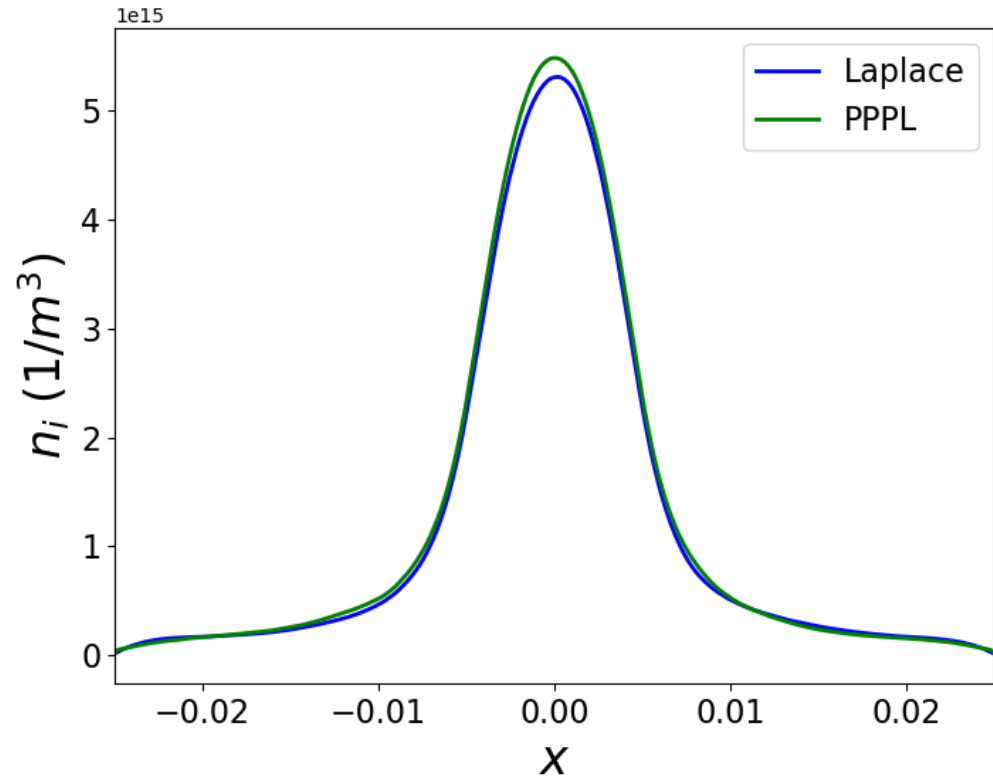


Penning discharge benchmark simulation schematic

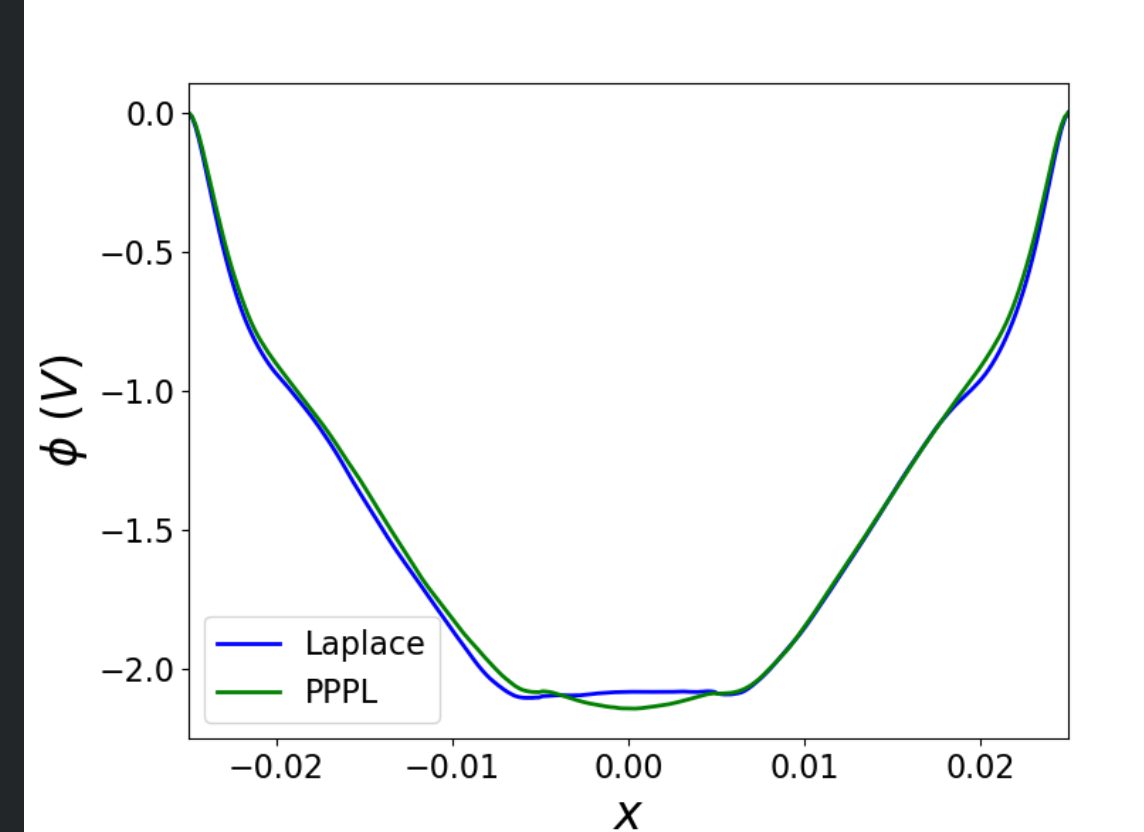


Total electrons and ions vs time within the entire simulation domain

Results – Time Averaged Cross-Section Profiles



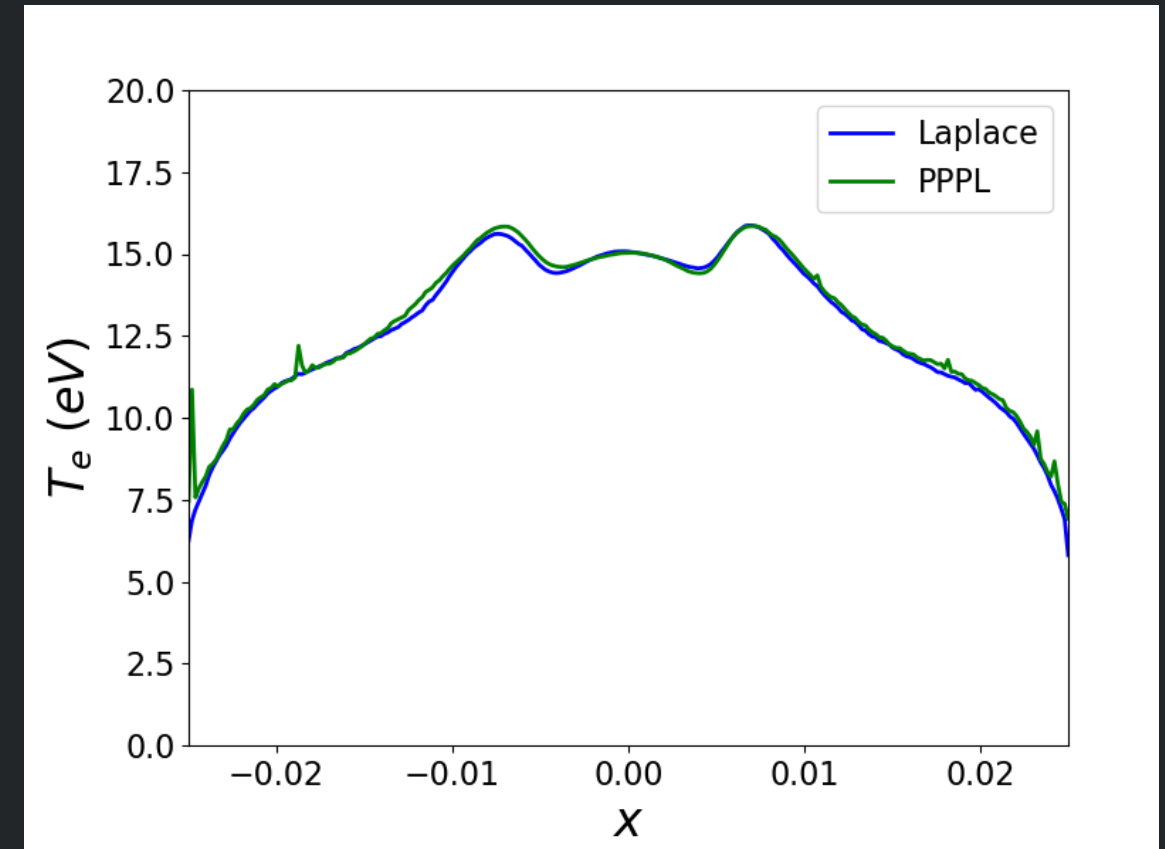
Cross-section and temporal average of ion density



Cross-section and temporal average of plasma potential

Results – Time Averaged Cross-Section Profiles

- One issue with this simulation is that there are very large changes in density from within to outside the spoke
- With fixed macroparticle weight, this leads to some regions with very poor statistics (i.e. outside the spoke near the boundary)
- As such, how we perform the time averaging of temperature can make a difference in the results



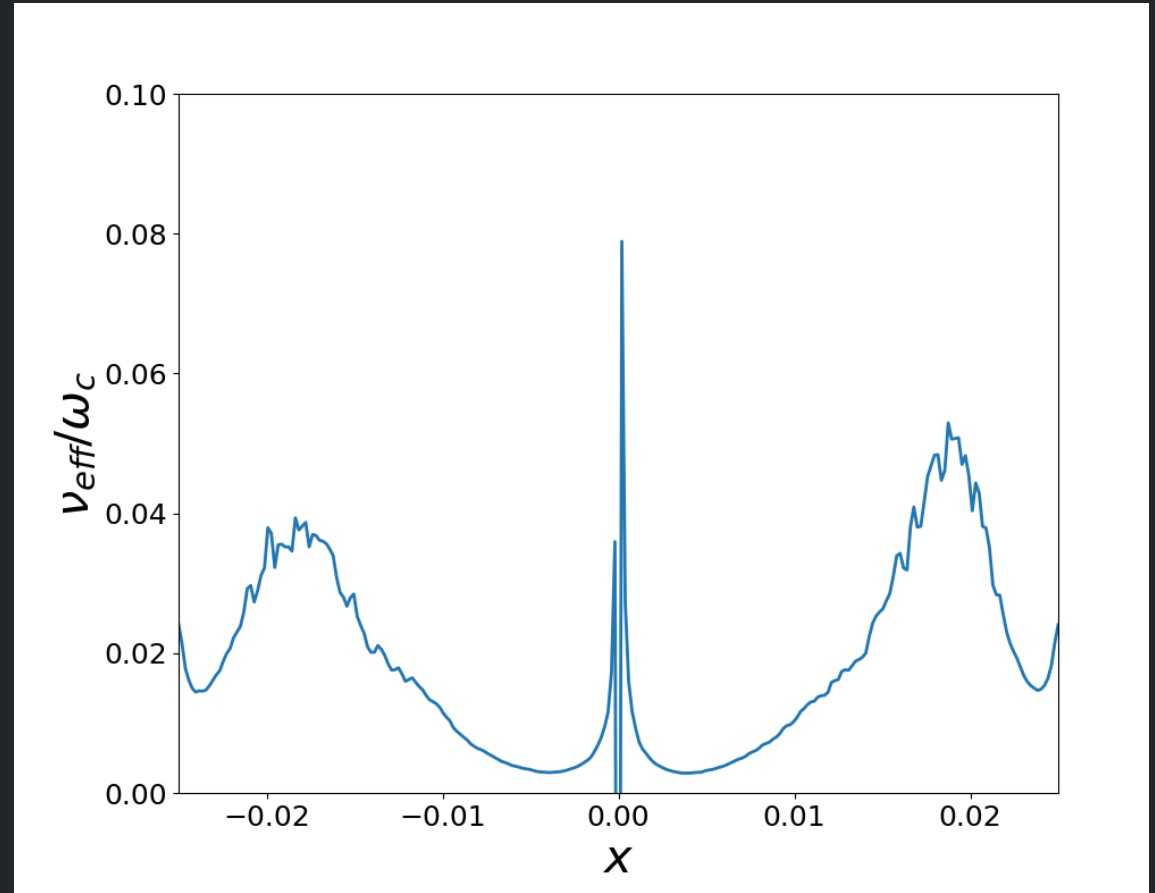
Cross-section and temporal average of electron temperature

Results – Time Averaged Cross-Section Profiles

- We derive an effective collision frequency for the radially transported electrons from the steady state electron continuity and momentum equations

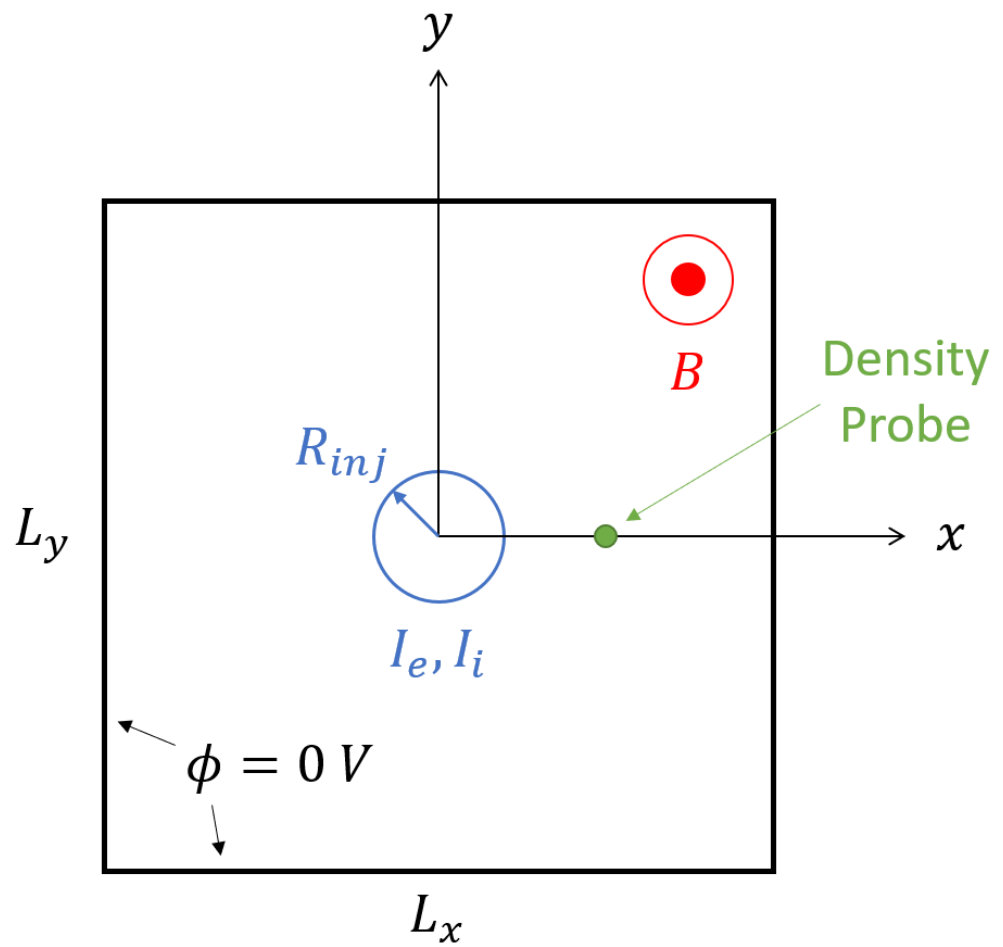
$$\nu_{eff}(r) = j_r(r) \frac{B^2}{m_e} \left[\frac{1}{e} \frac{\partial P(r)}{\partial r} + n(r) E_r(r) \right]^{-1}$$

- Since this equation involves the temperature (through pressure) we suffer from similar statistic issues when time averaging
- This is exacerbated by having a small denominator near in regions near the simulation boundary
- Clearly this result is non-symmetrical and highly noisy
- It's an interesting physical result, but is it worth keeping?

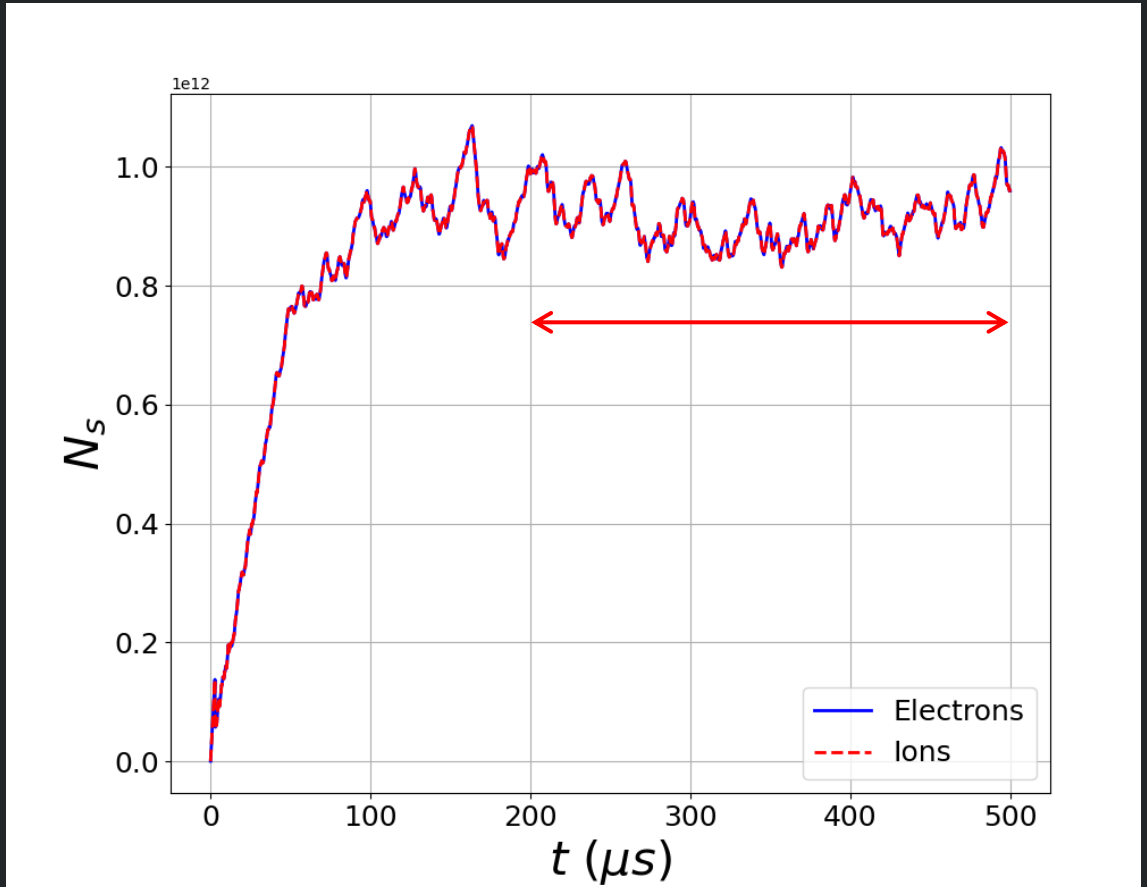


Cross-section and temporal average of effective radial electron collision frequency

Diagnostics – Spoke Frequency



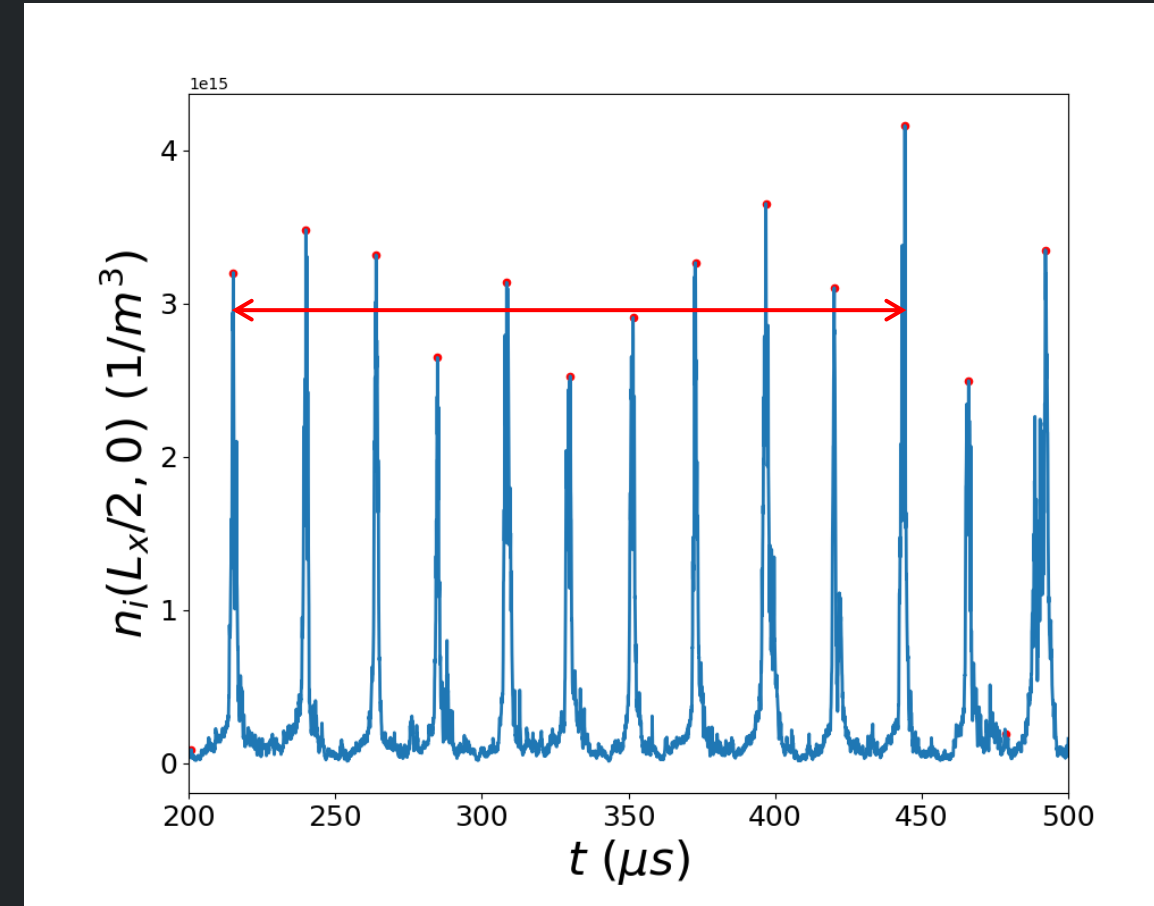
Penning discharge benchmark simulation schematic



Total electrons and ions vs time within the entire simulation domain

Diagnostics – Spoke Frequency

- Plot density at $x = L_x/2, y = 0$ against time
- Compute the spoke period by averaging over the first 10 peaks
- Gives a frequency of 45.60 kHz



Ion density vs time at probe location

Next Steps

Questions to answer:

- How do we perform time-averaging of temperature and effective collision frequency?
- Are there any other diagnostics which should be included?

Collisional Simulations

- Propose to begin with electron-neutral elastic and ionization collisions
- Incorporate excitation as well as ion-neutral collisions
- Do we need coulomb collisions?

Continue discussions with experimentalists on an appropriate experimental setup which is achievable with modern codes

Expressions of Interest

- **LPP** – Anne Bourdon, Federico Petronio, Alejandro Alvarez-Laguna
- **CERFACS** – Benedicte Cuenot, Olivier Vermorel, Gabriel Vigot
- **Princeton/PPPL** – Andrew (Tasman) Powis, Igor Kaganovich, Willca Villafana
- **Saskastchewan** – Dmytro Sydorenko, Andrei Smolyakov
- **Laplace** – Laurent Garrigues, Gwenael Fubiani
- **CNR-Bari** – Francesco Taccogna, Filippo Cichocki
- **Bochum** – Denis Eremin
- **Stanford** – Ken Hara
- **Onera** – Paul Quentin Elias
- **Madrid** – Eduardo Ahedo, Mario Merino, Enrique Bello Benitez, Alberto Marin Cebrian
- **JIHT RAS** – Timofey Chernyshev
- **Wigner Research Center for Physics** – Peter Hartmann, Zoltan Donko
- **Dublin City University** – Miles Turner
- **VKI-Bruxelles** – Thierry Magin, Pietro Parodi
- **Imperial College** – Aaron Knoll, Maryam Reza

How to get involved

- Contact us!
 - Andrew (Tasman) Powis – **apowis@pppl.gov**
 - Laurent Garrigues - **laurent.garrigues@laplace.univ-tlse.fr**
- Request to join our Slack channel: **landmark-benchmark.slack.com**
- We also highly encourage feedback on both the problem itself and the process of the benchmarking effort

Spoke Simulation References

1. Sengupta, M., Smolyakov, A., & Raitses, Y. (2021). Restructuring of rotating spokes in response to changes in the radial electric field and the neutral pressure of a cylindrical magnetron plasma. *Journal of Applied Physics*, 129(22), 223302.
2. Boeuf, J. P., & Takahashi, M. (2020). Rotating spokes, ionization instability, and electron vortices in partially magnetized E×B plasmas. *Physical review letters*, 124(18), 185005.
3. Koshkarov, O., Smolyakov, A., Raitses, Y., & Kaganovich, I. (2019). Erratum: Self-Organization, Structures, and Anomalous Transport in Turbulent Partially Magnetized Plasmas with Crossed Electric and Magnetic Fields [Phys. Rev. Lett. 122, 185001 (2019)]. *Physical Review Letters*, 123(23), 239903.
4. Matyash, K., Schneider, R., Mazouffre, S., Tsikata, S., & Grimaud, L. (2019). Rotating spoke instabilities in a wall-less Hall thruster: Simulations. *Plasma Sources Science and Technology*, 28(4), 044002.
5. Boeuf, J. P. (2019). Micro instabilities and rotating spokes in the near-anode region of partially magnetized plasmas. *Physics of Plasmas*, 26(7), 072113.
6. Powis, A. T., Carlsson, J. A., Kaganovich, I. D., Raitses, Y., & Smolyakov, A. (2018). Scaling of spoke rotation frequency within a Penning discharge. *Physics of Plasmas*, 25(7), 072110.
7. Taccogna, F., & Minelli, P. (2018). Three-dimensional particle-in-cell model of Hall thruster: The discharge channel. *Physics of Plasmas*, 25(6), 061208.
8. Kawashima, R., Hara, K., & Komurasaki, K. (2018). Numerical analysis of azimuthal rotating spokes in a crossed-field discharge plasma. *Plasma Sources Science and Technology*, 27(3), 035010.
9. Boeuf, J. P., & Chaudhury, B. (2013). Rotating instability in low-temperature magnetized plasmas. *Physical review letters*, 111(15), 155005.

Experimental References – Penning Like

Penning like and plasma columns

10. Gonzalez-Fernandez, V., David, P., Baude, R., Escarguel, A., & Camenen, Y. (2020). Spatially resolved determination of the electronic density and temperature by a visible spectro-tomography diagnostic in a linear magnetized plasma. *Scientific Reports*, 10(1), 1-12.
11. Rodríguez, E., Skoutnev, V., Raitses, Y., Powis, A., Kaganovich, I., & Smolyakov, A. (2019). Boundary-induced effect on the spoke-like activity in $E \times B$ plasma. *Physics of Plasmas*, 26(5), 053503.
12. Claire, N., Escarguel, A., Rebont, C., & Doveil, F. (2018). Ion velocity analysis of rotating structures in a magnetic linear plasma device. *Physics of Plasmas*, 25(6), 061203.
13. Raitses, Y., Kaganovich, I., & Smolyakov, A. (2015, July). Effects of the gas pressure on low frequency oscillations in $e \times b$ discharges. In *Proceedings of the Joint Conference of 30th ISTS, 34th IEPC, and 6th NSAT*.
14. Sakawa, Y., Joshi, C., Kaw, P. K., Chen, F. F., & Jain, V. K. (1993). Excitation of the modified Simon–Hoh instability in an electron beam produced plasma. *Physics of Fluids B: Plasma Physics*, 5(6), 1681-1694.
15. Thomassen, K. I. (1966). Turbulent diffusion in a Penning-type discharge. *The Physics of Fluids*, 9(9), 1836-1842.

Experimental References – Hall Thrusters

Hall Thrusters

16. Mazouffre, S., Grimaud, L., Tsikata, S., Matyash, K., & Schneider, R. (2019). Rotating spoke instabilities in a wall-less Hall thruster: Experiments. *Plasma Sources Science and Technology*, 28(5), 054002.
17. Hyatt, N. (2017). Hall effect thruster characterization through potential, magnetic, and optical measurements. In *55th AIAA Aerospace Sciences Meeting* (p. 0169).
18. Cappelli, M., Raitses, Y., & Kaganovich, I. (2016). *Coherent structures in plasmas relevant to electric propulsion*. Board of Trustees of the Leland Stanford Junior University Palo Alto United States.
19. Liu, D., Huffman, R. E., Branam, R. D., & Hargus, W. A. (2014). Ultrahigh speed images of hall thruster azimuthal instabilities. *IEEE Transactions on Plasma Science*, 42(10), 2656-2657.
20. Sekerak, M. J., Longmier, B. W., Gallimore, A. D., Brown, D. L., Hofer, R. R., & Polk, J. E. (2014). Azimuthal spoke propagation in Hall effect thrusters. *IEEE Transactions on Plasma Science*, 43(1), 72-85.
21. Ellison, C. L., Raitses, Y., & Fisch, N. J. (2012). Cross-field electron transport induced by a rotating spoke in a cylindrical Hall thruster. *Physics of Plasmas*, 19(1), 013503.
22. Griswold, M. E., Ellison, C. L., Raitses, Y., & Fisch, N. J. (2012). Feedback control of an azimuthal oscillation in the $E \times B$ discharge of Hall thrusters. *Physics of Plasmas*, 19(5), 053506.
23. Raitses, Y., Griswold, M., Ellison, L., Parker, J., & Fisch, N. (2012, December). Studies of rotating spoke oscillations in cylindrical hall thrusters. In *48th AIAA/ASME/SAE/ASEE Joint Propulsion Conference & Exhibit* (p. 4179).
24. Ellison, L., Raitses, Y., & Fisch, N. J. (2011, September). Direct measurement of spoke-induced, cross-field electron transport in a cylindrical Hall thruster. In *32nd International Electric Propulsion Conference (Wiesbaden, Germany)* (pp. 11-15).
25. McDonald, M. S., & Gallimore, A. D. (2011). Rotating spoke instabilities in Hall thrusters. *IEEE Transactions on Plasma Science*, 39(11), 2952-2953.
26. Parker, J. B., Raitses, Y., & Fisch, N. J. (2010). Transition in electron transport in a cylindrical Hall thruster. *Applied Physics Letters*, 97(9), 091501.
27. Esipchuk, Y. B., Morozov, A. I., Tilinin, G. N., & Trofimov, A. V. (1974). Plasma oscillations in closed-drift accelerators with an extended acceleration zone. *Soviet Physics Technical Physics*, 18, 928.
28. Janes, G. S., & Lowder, R. S. (1966). Anomalous electron diffusion and ion acceleration in a low-density plasma. *The Physics of Fluids*, 9(6), 1115-1123.

Experimental References - Magnetrons

Planar Magnetrons

29. Hnilica, J., Klein, P., Šlapanská, M., Fekete, M., & Vašina, P. (2018). Effect of magnetic field on spoke behaviour in HiPIMS plasma. *Journal of Physics D: Applied Physics*, 51(9), 095204.
30. Anders, A., & Yang, Y. (2017). Direct observation of spoke evolution in magnetron sputtering. *Applied Physics Letters*, 111(6), 064103.
31. Hecimovic, A., Britun, N., Konstantinidis, S., & Snyders, R. (2017). Sputtering process in the presence of plasma self-organization. *Applied Physics Letters*, 110(1), 014103.
32. Panjan, M., & Anders, A. (2017). Plasma potential of a moving ionization zone in DC magnetron sputtering. *Journal of Applied Physics*, 121(6), 063302.
33. Hecimovic, A., Schulz-von der Gathen, V., Böke, M., Von Keudell, A., & Winter, J. (2015). Spoke transitions in HiPIMS discharges. *Plasma Sources Science and Technology*, 24(4), 045005.
34. Poolcharuansin, P., Estrin, F. L., & Bradley, J. W. (2015). The use of segmented cathodes to determine the spoke current density distribution in high power impulse magnetron sputtering plasmas. *Journal of Applied Physics*, 117(16), 163304.
35. Winter, J., Hecimovic, A., De los Arcos, T., Böke, M., & Schulz-Von Der Gathen, V. (2013). Instabilities in high-power impulse magnetron plasmas: from stochasticity to periodicity. *Journal of Physics D: Applied Physics*, 46(8), 084007.
36. Anders, A., Ni, P., & Rauch, A. (2012). Drifting localization of ionization runaway: Unraveling the nature of anomalous transport in high power impulse magnetron sputtering. *Journal of Applied Physics*, 111(5), 053304.

Cylindrical Magnetrons

37. Brenning, N., Lundin, D., Minea, T., Costin, C., & Vitelaru, C. (2013). Spokes and charged particle transport in HiPIMS magnetrons. *Journal of Physics D: Applied Physics*, 46(8), 084005.
38. Eriasarian, A. P., Hecimovic, A., De Los Arcos, T., New, R., Schulz-von der Gathen, V., Böke, M., & Winter, J. (2012). High power impulse magnetron sputtering discharges: Instabilities and plasma self-organization. *Applied Physics Letters*, 100(11), 114101.

Discussion: validation of PIC simulations